Assessment of tropospheric ozone products from CAMS reanalysis and near-real time analysis using observations over Iran

Najmeh Kaffashzadeh[1] and Abbas Ali Aliakbari Bidokhti[1]

[1] Institute of Geophysics, University of Tehran, Tehran, Iran

5   *Correspondence to*: Kaffashzadeh Najmeh (n.kaffashzadeh@ut.ac.ir)

Abstract. Tropospheric ozone time series consists of the effects of various scales of motion, from meso to large time scales which is often challenging for global models to capture them. This study uses two global datasets, namely reanalysis and analysis of the Copernicus atmospheric Monitoring Service (CAMS), to assess the capability of these models or systems in presenting ozone's features in small scales. We employ the tropospheric ozone product of the models and in situ measurements

10   at 18 stations over Iran for the year of 2020. Furthermore, we make use of data of ozone, temperature, nitrogen oxides, wind speed, and wind direction at one more station. We decompose the datasets into three spectral components, i.e., short (S), medium (M), and long (L) term. We only evaluate the S and M terms of modelled against those of observed datasets for all stations. We examine the relationship between ozone and the relevant proxies. Results show a correlation coefficient of larger than 0.5 for S and about 0.25 for M term in both models. It turns out that the reanalysis dataset demonstrates more precision

15   for the S component than that for the M. Both models can show the observed correlation between ozone and temperature, whereas some inconsistencies appear in presenting the anti-correlation between ozone and nitrogen oxides.

1 Introduction

Near surface ozone (O_3), or tropospheric ozone at the ground level, is a secondary air pollutant that deteriorates human health and plants via damaging respiratory systems (Bell et al., 2006; Fowler et al., 2009; Mills et al., 2011; Malley et al., 2015).

20   Surface ozone is either transported naturally from the stratosphere or produced in situ by photochemical oxidation of ozone's precursor gases such as nitrogen oxides, non-methane volatile organic compounds, methane or carbon monoxide in the presence of sunlight (Crutzen 1974; Monks et al., 2015; Cooper et al., 2014). The ozone level is not only a function of its precursor's emissions, but also meteorological conditions that influence the evolution of emissions and photochemical products (Bloomer et al., 2009; Li et al., 2020).

25   Global chemistry climate models, as a tool that the user can rely on, provide an estimation of the radiative forcing of tropospheric ozone from preindustrial period to the present and project this variation into the future in a global scale (Stevenson et al., 2006; Murazaki and Hess, 2006; Lin et al., 2008a). These models have been widely used as an initial condition for the daily forecast of the atmosphere or boundary conditions in regional models, and as proxies to complement insufficient in situ measurements. Often these models contain coarse grid boxes, i.e., 100 km, which prevent an adequate representation of

30   mesoscale meteorology cyclone wave activity that leads to uncertainty in ozone precursor's transportation (Lin et al., 2008b). The mesoscale events such as land-sea breezes and topographically forced flows determine whether ozone precursor species remain locally or transport downwind. Representation of mesoscale circulations associated with cyclones could be achieved with a resolution less than 0.25°.

Iran is a country with a complex topography and diverse meteorological systems as it extends from about 25° N to nearly 40°
35   N latitude. Many efforts have been done to study ozone and its precursors over this country (Lelieveld et al., 2009; Bidokhti et al., 2016; Faridi et al., 2018; Yousefian et al., 2020). Most of the studies have been conducted over Tehran megacity, which suffers from severe ambient air pollutions (Zohdirad et al., 2020; Borhani et al., 2021; Jafari Hombari and Pazhoh, 2022). They have shown that not only local emissions and winds, but also synoptic conditions control the ozone levels. Synoptic systems, which cause to high level of ozone, over Tehran has been classified in a study by Khansalari et al. (2020) and Lashkari et al.
40   (2020). Taking into account of the complex topography of the country and the contribution of various factors in different time scales on ozone: can we use global models data to study the surface ozone over Iran? Or which global models are (more) suitable for the study of ozone over this country?

To answer these questions, we select two types of global models' data. The first is a global model that is assimilated by various observations such as satellite, radar, and in situ measurements, that is called reanalysis. The latter is a global model with a fine
45   resolution and the large number of vertical levels that can resolve the orography. We use measured ozone data at 19 stations for the year of 2020, in which the second model data has been available with the required resolution. To assess ozone in each time scales, i.e., meso, synoptic or large scale, the observed and modelled datasets are decomposed to three spectral components. Then the models' performances are evaluated and compared for each spectral component. Relationships between ozone data and a few relevant proxies are quantified for the observations and models datasets that identify the models'
50   capability in representing these relationships.

A detail description of the datasets (observations and models) used in this study is presented in Sect. 2. Methodology is explained in Sect. 3 and the results are shown in Sect. 4. Discussion is presented in Sect. 5 and the paper ends with conclusion' remarks in Sect. 6.

2 Description of Data

55   **2.1 Models**

2.1.1 CAMS reanalysis

The Copernicus Atmosphere Monitoring Service (CAMS) has been developed in recent years to assimilate the chemical compositions such as tropospheric ozone and aerosol concentrations, but it also holds outputs for several meteorological variables (Innes et al., 2019). The CAMS product is the latest (state-of-the-art) global reanalysis datasets of atmospheric
60   compositions. It is noteworthy that newer versions of data have been frequently adopted in CAMS. Comparing to the previous

atmospheric chemistry reanalysis data, CAMS has a finer horizontal resolution of 80 km with 60 vertical levels. CAMS covers data for the period of the January 2003 to June 2020. The data are archived in 3 hourly time intervals. Several studies have evaluated CAMS products and compared them with other reanalysis datasets and control run (no assimilation). As an example, an inter-comparison of tropospheric ozone from seven reanalysis datasets in East Asia has reported that CAMS depicts more

65   reasonable spatial-temporal variability than other datasets (Park et al., 2020). They also show the suitability of CAMS for the study of local tropospheric ozone on seasonal to interannual time scales, but inadequacy of that to study trend (long-term). Despite the well performance of CAMS in upper troposphere, it shows bias at the surface for many parts of the globe (Wang et al., 2020). Meanwhile, several of these studies mention that the performance of CAMS differs depending on the region. For instance, it has been shown more agreement between CAMS and observations over Europe than Tropics (Errera et al., 2021).

70   **2.1.2 CAMS near real-time analysis**

In addition to aforementioned datasets, CAMS provides global (near real-time) forecasts, called analysis, of various chemical compositions and meteorological variables twice a day. In contrast to the reanalysis datasets, the forecast data are available on a finer resolution of 40 km. This system is upgraded regularly, e.g., once a year, in which model's resolution can change or new species can be added. On July 2019 the model vertical levels have been upgraded from 60 to 137. The temporal coverage

75   of the data is from 2015 to present with temporal resolution of 1 hourly and 3 hourly (within five forecasts days). System's upgrades and its verification are reported in several studies (Shulz et al., 2021; Eskes et al., 2021). A recent validation based on various observations shows that, in terms of bias, analysis overestimates surface ozone values at most of the stations (Sudarchikova et al., 2021). However, it shows a significant correlation over most of the stations, e.g., in China.

2.2 In situ measurement datasets

80   Surface based measurements of ozone were extracted from Tehran air quality control portal for 19 stations. Hourly time series of surface ozone were obtained from Iran Environmental Protection organization for eight additional stations. We add Geophysics station, which contains not only data for ozone but also for a few proxies such as air temperature, nitrogen oxides, and wind. To have a common quality, validity of the data was checked by performing a few statistical tests such as range, constant values, and missing value tests suggested in literatures (Zurbenko et al., 1996; Zahumensky, 2004; Gerharz et al.,

85   2011; Taylor and Loescher, 2013). The invalid values were majorly flagged in the missing values test, which identifies suspicious data points before and ahead of the discontinuities. We use the stations containing data for the year of 2020, where more than 50 percent of the data are available for each month. Table A1 lists the names and geographical locations of the stations, which are ordered based on the stations' latitudes. In this table, there is a number along with the stations' name, hereafter, the stations are referred with these numbers.

90   Hereafter, the observation, reanalysis and analysis datasets are called as dfo, dfr, and dfa, respectively.

3 Methodology

Observed data are available in hourly resolution, in contrast to the model values that are available in 3 hourly intervals. To match the frequency of the model outputs with observations, 3 hourly observed values are considered in such a way that at least two hourly values are available, otherwise it renders the value as a missing data. The vertical model level at each station

95 location was selected based on the minimum difference between the station altitude and the central altitude of the model level obtained when converting model level pressure to altitude with the barometric equation and using a scale height of 7640 m. For surface pressure, the annual average surface pressure of the grid box was used.

3.1 Spectral decomposition of the time series

The presence of various scales of motions, which caused by several physical and chemical processes, in time series of O_3 can

100 complicate analysis and interpretation of data. As an example, short-term and fast fluctuations in O_3 time series are majorly attributed to the chemical process such as NO titration, whereas long-term and seasonal variation is mainly related to the solar radiation. Scale analysis is a method by which the time series can separate into different temporal terms. Here, the time series of O_3 is decomposed into three different spectral components, namely short (period less than 2 days), medium (period of 2-21 days), and long (periods longer than 21 days) terms by applying Kolmogorov-Zurbenko (KZ) technique (Rao et al., 1997). KZ

105 is essentially a low pass filter, which consists of repeated moving average. Its use has been demonstrated in earlier studies (Hogrefe et al., 2000, 2014; Kang et al., 2013; Seo et al., 2014). A detailed discussion of the KZ filter along with the comparison to other separation techniques can be found in Eskridge et al. (1998) and Loneck and Zurbenko (2020). KZ requires two input parameters, KZ (m, k), where m is the window size for filtering and k is the number of iterations. Since the values that have been commonly used for m and k in the literature may not be applicable for 3 hourly data, we selected them based on the

110 criterion suggested in Yang and Zurbenko (2010):

$$m \times \sqrt{k} \leq p \tag{1}$$

KZ filters out all periods that are less than p. Therefore, three components of interest in this study are estimated as following:

$$S = O - KZ (5, 5) \tag{2}$$

$$M = KZ (5, 5) – KZ (35, 5) \tag{3}$$

115 $$L = KZ (35, 5) \tag{4}$$

where O refers to the original time series and S, M, and L indicate the short, medium, and long terms, respectively.

3.2 Model evaluation

We use the mean square error (MSE) as a metrics to evaluate the models' performance. The MSE is defined as the squared mean of the difference between modelled (x_m) and observed (x_o) variables.

120 This metric can be modified to include all relevant model evaluation indicators, i.e., bias, variance, and correlation, as (Murphy, 1988; Solazzo and Galmarini, 2016):

$$MSE = (\bar{x}_m - \bar{x}_o)^2 + (\sigma_m - r\,\sigma_o)^2 + \sigma_o^2(1 - r^2) \qquad (5)$$

where σ_m and σ_o refer to the standard deviation of the modelled and observed data respectively, and r is the coefficient of correlation between the observed and assimilated datasets. In Eq. (5), the first term (hereafter e_1) shows the deviation between

125 average modelled ($\bar{x}_m$) and measured ($\bar{x}_o$) datasets and refers to the model accuracy. The second term (hereafter e_2) contains the variance error, i.e., the discrepancy in amplitude or phase between the variability of the modelled and observed values, that determines the precision of the model. Also, the third part (hereafter e_3) refers to unsystematic errors related to the associativity between observed and assimilated datasets. In other words, the e_2 indicates an explained error which reveals the variance error arising from the variability of the modelled variables not observed in measurements. The e_3 represents an unexplained error

130 reflecting the lack of observed variability in the modelled data. Due to the spectral decomposition of the data, the S and M components are zero-mean fluctuations. Hence, the e_1 term in Eq. (5) is zero and only the e_2 and e_3 terms are analysed below.

3.3 Multiple linear regressions

To find a quantitative relationship between variability of O_3 and several predictors, a multiple linear regression (MLR) is defined as:

135 $$O_3(t) \approx a_0 + a_1\,NO_x(t) + a_2\,AT(t) + a_3\,WS(t) + a_4\,WD(t) \qquad (6)$$

where a_0 is an intercept, a_1, a_2, a_3, and a_4 are the regression coefficients for NO_x (nitrogen oxides), AT (temperature), WS (wind speed), and WD (wind direction). These predictors are relevant proxies for the regression model of O_3 (Bloomfield et al., 1996; Abdul-Wahab et al., 2005; Rasmussen et al., 2012; Otero et al., 2018). In order to allow comparison between the regression coefficients of the different variables, the MLR is performed over standardized data, i.e., mean 0 and standard deviation of 1,

140 for both S and M components.

4 Results

The time series of O_3 and all meteorological variables for observations and models decompose into three spectral, short (S), medium (M), and long (L), by applying the method (KZ filter) explained in Sect. 3.1.

Figure 1 shows the original O_3 time series of observations and two models and its estimated spectral components at first station.

145 To clearly see the signals, we only show part of the time series, here the summer month (June, July, and August: JJA). Looking at the original 3 hourly times series (a), both models overestimate and underestimate ozone during different periods, but it is difficult to determine any clear patterns or identify specific reasons for the model bias. The S component contains frequent fast oscillations occurring every day with regular maxima and minima (see panel (b) in Fig. 1). In this figure, the amplitude of S oscillations in the two models is different from that in dfo, indicating differences in the diurnal cycle of observed and

150 simulated ozone mixing ratios. The M term captures variability on the time scale of synoptic systems. Some episodic events

are more visible in the M component than in S. For instance, in panel (c) of Fig. 1, the M component of the observation represents a clear signal of an episodic event in middle of June. This episode is not well captured in dfr while they are captured by dfa. It seems for most of the periods the variations of M component in both models are in good agreement with those in observations while the amplitudes of oscillations in the models do not correspond well with that of the observations. The

155   underestimation and overestimation of the amplitude (with respect to observations) in dfa is less than that in dfr. Compared to S and M terms, which oscillate around zero, the mean values of the L components are not zero (see panel (d) in Fig. 1). L represents variations of the ozone mixing ratios on seasonal, semi-seasonal, and multi-annual time scales. Comparing the variations of dfr and dfa with dfo for L shows more similarity between dfa and dfo than between dfr and dfo. Both models exhibit a high bias with respect to the ozone mixing ratios. Nevertheless, the decomposition of L component is not reliable due

160   to limited period (one year) of the available data, so hereafter we only assess the S and M components.

Figure 2 shows the box plots of MSE and different terms of MSE, i.e., e_2, e_3, for O_3 simulation in both components. From panel (a) in Fig. 2, it turns out the mean MSE (shown with red squares) of O_3 for S component is larger than for M component for both models. In other words, there is a better agreement between M components of observations and models than S components. That arises from larger variability of S than M (see Fig. 1). The mean of MSE in dfr for S component (dfr_s) is

165   larger than that in dfa (dfa_s). Whereas, for the M component the differences between MSE of dfr and dfa is less. So, S consists of more variability in dfr than that in dfa. Panel (b) in Fig. 2 shows the explained error (e_2) in dfr and dfa for both components. The higher e_2 for S in comparison to that for M component can contribute to the large MSE of S. Since e_2 is a model related error, a possible source for the large e_2 of S can be the misrepresentation of short and meso scale phenomena in models. As can be seen in the model with a higher resolution, i.e., dfa, this error is less than that in dfr. This error could also arise from

170   the assimilated processes which causes a larger variability in dfr than dfa. The unexplained error (e_3) for both components is presented in panel (c) of Fig. 2. Similar to e_2, the e_3 for S component is larger than that for M as expected from the variance of these components. Large value of e_3 for S component can arise from the models' deficiency in resolving the meso-scale phenomena such as local winds, NO titration and their influences on O_3 variability.

Assessing the element of e_2 (see second term of Eq. (5)) shows that the large variance of the model (σ_m), small variance of

175   observations (σ_o), or small correlation (r) causes the large e_2 and consequently large MSE. Panel (a) of Fig. A1 shows the correlation between the models and observation datasets for both components. This figure shows that the S contains a larger correlation (r > 0.5) than M (r ≈ 0.25) in both models. In addition, the mean value of correlation ($\bar{r}$) for the S component of dfr (= 0.62) is larger than that for dfa (= 0.51), while for the M of dfr and dfa it ($\bar{r}$) is 0.19 and 0.22, respectively. A high value of correlation between two terms can be attributed to the larger covariance of two terms or less variance of each term. panel

180   (b) of Fig. A1 shows the covariance between models and observations. As can be seen in this figure, the covariance between dfr and dfo (= 407.01) is much larger than that for dfa (= 97.5) for S component, while that is nearly the same for M. The S of dfr (dfr_s) shows larger variance than that of dfa (dfa_s), whereas its M component (dfr_m) contains less value than dfa (dfa_m) in panel (c) of Fig. A1. In this figure, the mean value of variance for dfa_s and df_m is close to that for dfo_s and

dfr_m, respectively. So, the high correlation is majorly attributed to the large covariance, and large value of e_2 is caused by the models' variance.

Four stations, i.e., 1, 2, 3, and 15, appear as fliers (see black circles in panel (a) of Fig. 2) with low value of MSE in dfr, less than 500 and 20 for S (dfr_s) and M (dfr_m), respectively. That arises from the low value of e_2 (see panel (b) in Fig. 2). A smaller correlation (and covariance) between simulated and observed O_3 are shown at these sites comparing to other stations (see circles for dfr_s in panel (a-b) of Fig. A1). Nevertheless, at these sites, the variances of dfr_s and df_m is less than other stations (panel (c) of Fig. A1). Thus, the small value of MSE at these stations is mainly attributed to the low model variabilities. The variabilities of the spectral components of the observed O_3, with respect to the relevant proxies, are quantified by using a MLR model explained in Sect. 3.3. Table 1 lists the regression coefficients a_i (i = 1...4) and coefficient of determination (R^2) for both components of observations at the station 8. Results of the regression coefficients in this table indicate a small difference between S and M for the regression coefficients of a_3 and a_4, however there is a large difference between a_1 and a_2, as predictors in S and those in M. For the S component, a_1 is -0.39 which means upon increasing NO_x by 1 unit (= 43.36 nmol mol^{-1}, see table A2), O_3 decreases by 0.39 units (= 18.11 nmol mol^{-1}, see table A2), holding other parameters constant. However, one unit change in M component of NO_x leads to a reduction of 0.34 unit of O_3 (= 4.88 nmol mol^{-1}, see table A3). Highest coefficient belongs to the AT (a_2 = 0.63) of the S component and indicates that the large association between short variabilities of AT and that of O_3. This association decreases to 0.23 for M. From the results in this table, it appears that the R^2 for the S is 0.67, while that is 0.2 for the M. This shows that the MLR model explains more variability of S than M.

Figure 3 shows regression coefficients and R^2 values for both S (a) and M (b) components of dfo, dfr, and dfa at station 8. While some coefficients span both positive and negative, a_2 is always positive (correlation). For instance, a_2 for S component of dfr and dfa are 0.71 and 0.81, which means upon increasing AT by 1 unit (= 2.69 °K of dfr and 2.88 °K of dfa, see table A2), O_3 increases by 0.71 units (= 31.9 nmol mol^{-1}, see table A2) in dfr and increase 0.81 units (= 15.46 nmol mol^{-1}, see table A2) in dfa. Although both dfr and dfa are in a good agreement with observations in presenting the positive correlation between O_3 and AT (see Fig. 3), the behavior of other predictors are highly variables. Similar to dfo, there is an anti-correlation between S component of O_3 and NO_x in dfr, while dfa shows a positive correlation. On the other hands, for M component dfr shows a correlation between O_3 and NO_x, whereas dfo and dfa show an anti-correlation. The negative association (anti-correlation) between O_3 and NO_x presented in dfo, is captured by S of dfr and M of dfa. In addition to the sign of coefficients in this figure, its absolute value is highly variable compared to a_2. It is clear that for dfo where $|a_1|$ value is high (= 0.39), it falls to 0.11 for dfr and to 0.15 for dfa. This shows a smaller contribution of NO_x to O_3 in models comparing to that of observations. R^2 for S component of dfr and dfa are 0.68 and 0.56, respectively, while for M that is 0.23 and 0.09. Smaller R^2 of dfa comparing to that of dfo indicates that the model parametrization yields a weaker relationship between predictors and O_3 than that in observations.

Geoscientific
Model Development
Discussions

5 Discussion

Analysis of the spectral components in this study reveals that the O_3 variabilities in both models possess a nearly similar shape (although in different phase and amplitude) as those in observations. Results of the models' performances show a larger MSE of S than that of M in both models. That arises from the larger variabilities of S in comparison to M (Hogrefe et al., 2000; Hogrefe et al., 2014). The results of error apportionment show that the MSE majorly has been arisen from the e_2, which emphasizes the modeling related error such as large models' variance. The e_2 assessment shows more variability for both component of O_3 in models than that in observations. That could arise from the complex chemical processes in the models or imbalanced among coupled components (Park et al., 2020). Large variance of dfr with respect to dfa and dfo can be attributed to the assimilation's procedures.

Larger correlation coefficient of S comparing to that of M reflects a better agreement between short-term variabilities of the models and observations than the synoptic term. That is attributed to the models' capability in simulating diurnal (24 hourly) cycles as has been shown for the dfr (Huijnen et al., 2020). Model to model differences in correlation coefficient is more pronounced in S, as the correlation of dfr is slightly larger than dfa. That can be related to the assimilation of ozone's precursors such as NO_2, which affects the O_3 in the short time scale.

At four stations, dfr shows less correlation with respect to other stations. Three of these stations are in city of Tabriz, in north western part of Iran, where is often affected from cyclonic activities (Asakereh and Khojasteh, 2021) and summer circulations over eastern Mediterranean region (Tyrlis et al., 2013). Although CAMS reanalysis captures the long-range transport processes and atmospheric background in the troposphere, it shows a lower skill over Mediterranean, in particular eastern part, compared to other regions (Errera et al., 2021).

Large MSE at some stations could arise from the selected vertical level. Figure A2 shows the O_3 time series for dfo and two vertical levels of dfa at station 4. The time series of dfo contains lots of fast daily fluctuations, which are not pronounced at the selected vertical model levels of dfa (lev = 123) as those in observations. Whereas, at the surface level (lev = 137) there is more matching between oscillations of dfa and that of dfo. To assess the sensitivity of results to the vertical level, the results of model performance was obtained for dfa when they are interpolated at the model level of 137 (Fig. A3 panel). At the new vertical model levels, the mean of MSE decreases from 202.07 to 162.34 for S component and from 42.45 to 21.1 for M component of dfa. In this case, similar to the results in Sect. 4, the MSE of S component is larger than that for M.

A positive correlation between O_3 and AT is shown for both components of all datasets. That is consistent with the results of other literatures (Ordóñez et al. 2005; Camalier et al., 2007; Otero et al., 2016; Otero et al., 2018) which show that the higher AT leads to higher O_3 through different processes. High AT leads to high photolysis rate and high concentration of O_3 precursors from dissociation of PAN, biogenic emission of isoprene, etc. The S component of observations shows the most significant correlation between O_3 and AT, which is attributed to the diurnal variation. Although both models capture the true relationship (correlation) between O_3 and AT with slight underestimation, the anti-correlation between O_3 and NO_x are not well captured by them.

As an example, the S component of dfa and the M component of dfr show a positive correlation between O_3 and NO_x, despite the anti-correlation between observed O_3 and NO_x. In the study by Wang et al. (2020), it has been shown that the peak values

250   of some species such as NOx and CO is underestimated in dfr. Wind can influence O_3 concentration near the surface in a different way. If the site acts as a (point) source of O_3, the increase of the wind speed disperses (dissolute) ozone more efficiently from that place. Conversely, if the ozone chemical budget at one station is negative, wind can transport (transfer) the ozone-rich air from polluted regions to that site; in this case O_3 correlate positively with the wind speed. Nevertheless, in this study, the low value of a_3 and a_4 might arise form a non-linear relationship between O_3 and winds or unresolved time

255   scales; mountainous area of Iran often leads to local mesoscale circulations that can influence these processes and change near surface ozone, especially in urban areas as Tabriz or Tehran (Soltanzadeh et al., 2011). A weak (insignificant) correlation between wind speed and ozone level has been reported in other studies (Dawson et al., 2007; Otero et al., 2018). Although the selected parameters in MLR explained 67 % variabilities of S, they could explain only 20 % of the M. This indicates the role of other parameters that are not included in the MLR. For instance, Kaffashzadeh (2018) showed that the relative humidity is

260   the most influential factor on the synoptic surface ozone variability over Mediterranean region.

6 Conclusions

In this paper, the variability of O_3 in two global models, namely reanalysis and analysis, was assessed against that in observations at 19 stations over Iran. We decomposed the O_3 times series of all datasets to three spectral components, i.e., short (S), medium (M) and long (L) terms. The S contains intraday and diurnal fluctuations, the M term include synoptic fluctuations

265   and the other fluctuation, i.e., seasonal, semi-seasonal, and trend, carries in L. We only assessed the S and M terms due to the availability of one year data, i.e., 2020; the L component is primarily used to check the biases between model data and observations, but should not be considered reliable with respect to trend analysis etc. Since S and M components have zero-mean fluctuations, the bias term (distance between time average of model data and observations) is zero, and the main focus of this study was to analyse the variability term, e.g., variance and covariance. To assess how some processes involved in the

270   observed O_3 variability, we make use of a few relevant proxies such as NO_x, AT, WD and WS as predictors in the MLR model. The results presented in this study reveal three key points: (1) the S component of both models shows larger correlation with observations than M term. This indicates a higher capability of models in simulating the S variability of ozone compared to the synoptic term. (2) To study the S variability of O_3, one should use the assimilated model data, which shows a high correlation with observed data. (3) Despite presenting the correlation between AT and O_3, the anti correlation between NO_x

275   and O_3 are not well captured in both models. That can be considered as a starting point to improve the results of tropospheric ozone, in particular at urban sites.

Code availability. The Python 3.7 code of the methodology will made be available to reader under Creative Common license on the GitHub repository of the corresponding author.

References

290   Abdul-Wahab S. A., Bakheit C. S., and Al-Alawi S. M.: Principal Component and Multiple Regression Analysis in Modelling
of Ground-Level Ozone and Factors Affecting its Concentrations, Environmental Modelling and Software, 20(10), 1263-1271,
doi: 10.1016/j.envsoft.2004.09.001, 2005.

Asakereh: Frequency of entrance Mediterranean Cyclones to Iran and Their Impact on Widespread precipitation,
2021.Murphy: skill score, 1988.Murazaki, K.: How does climate change contribute to surface ozone change over the United
295   States?, 111, 1–16, https://doi.org/10.1029/2005JD005873, 2006.

Bell, M. L., Peng, R. D., and Dominici, F.: The Exposure – Response Curve for Ozone and Risk of Mortality and the Adequacy
of Current Ozone Regulations, 532–536, https://doi.org/10.1289/ehp.8816, 2006.

Bidokhti, A. A., Shariepour, Z., and Sehatkashani, S.: Some resilient aspects of urban area to air pollution and climate change,
case study: tehran, Iran, 23, 1994–2005, 2016.

300   Bloomer, B. J., Stehr, J. W., Piety, C. A., Salawitch, R. J., and Dickerson, R. R.: Observed relationships of ozone air pollution
with temperature and emissions, 36, 1–5, https://doi.org/10.1029/2009GL037308, 2009.

Bloomfield, P. J., Royle, J. A., Steinberg, L. J., and Yang, Q.: Accounting for meteorological effects in measuring urban ozone
levels and trends, Atmos. Environ., 30, 3067–3077, https://doi.org/10.1016/1352-2310(95)00347-9, 1996.

Borhani, F., Shafiepour Motlagh, M., Stohl, A., Rashidi, Y., and Ehsani, A. H.: Tropospheric Ozone in Tehran, Iran, during
305   the last 20 years, Environ. Geochem. Health, 4, https://doi.org/10.1007/s10653-021-01117-4, 2021.

Camalier, L., Cox, W., and Dolwick, P.: The effects of meteorology on ozone in urban areas and their use in assessing ozone
trends, Atmospheric Environment, 41, 33, 7127-7137, https://doi.org/10.1016/j.atmosenv.2007.04.061, 2007.

Geoscientific
Model Development
Discussions

Cooper, O. R., Gilge, S., and Shindell, D. T.: Global distribution and trends of tropospheric ozone: An observation-based review, 1–28, https://doi.org/10.12952/journal.elementa.000029, 2014.

310 Crutzen, P. J.: Photochemical reactions initiated by and influencing ozone in unpolluted tropospheric air, 26, 47–57, https://doi.org/10.3402/tellusa.v26i1-2.9736, 1974.

Errera, Q., Y. Bennouna, M. Schulz, H.J. Eskes, S. Basart, A. Benedictow, A.-M. Blechschmidt, S. Chabrillat, H. Clark, E. Cuevas, H. Flentje, K.M. Hansen, U. Im, J. Kapsomenakis, B. Langerock, K. Petersen, A. Richter, N. Sudarchikova, V. Thouret, A. Wagner, Y. Wang, T. Warneke, C. Zerefos, Validation report of the CAMS global Reanalysis of aerosols and

315 reactive gases, years 2003-2020, Copernicus Atmosphere Monitoring Service (CAMS) report, CAMS84_2018SC3_D5.1.1-2020.pdf, doi:10.24380/8gf9-k005, 206 pp., June 2021.

Eskes, H. J., S. Basart, A. Benedictow, Y. Bennouna, A.-M. Blechschmidt, Q. Errera, K. M. Hansen, J. Kapsomenakis, B. Langerock, A. Richter, N. Sudarchikova, M. Schulz, C. Zerefos, Upgrade verification note for the CAMS near-real time global atmospheric composition service: Evaluation of the e-suite for the CAMS 47R3 upgrade of 12 October 2021, Copernicus

320 Atmosphere Monitoring Service (CAMS) report, CAMS84_2018SC3_D3.2.1-202109_esuite.pdf, doi:10.24380/hfvp-fq98, 91 pp., October 2021.

Eskridge, R. E., Ku, J. Y., Rao, S. T., Porter, P. S., and Zurbenko, I. G.: Separating Different Scales of Motion in Time Series of Meteorological Variables, 1473–1484, 1997.

Faridi, S., Shamsipour, M., Krzyzanowski, M., Künzli, N., Amini, H., Azimi, F., Malkawi, M., Momeniha, F., Gholampour,

325 A., Hassanvand, M. S., and Naddafi, K.: Long-term trends and health impact of PM2.5 and O3 in Tehran, Iran, 2006–2015, Environ. Int., 114, 37–49, https://doi.org/10.1016/j.envint.2018.02.026, 2018.

Fowler, D., Pilegaard, K., Sutton, M. A., Ambus, P., Raivonen, M., Duyzer, J., Simpson, D., Fagerli, H., Fuzzi, S., Schjoerring, J. K., Granier, C., Neftel, A., Isaksen, I. S. A., Laj, P., Maione, M., Monks, P. S., Burkhardt, J., Daemmgen, U., Neirynck, J., Per- sonne, E., Wichink-Kruit, R., Butterbach-Bahl, K., Flechard, C., Tuovinen, J. P., Coyle, M., Gerosa, G., Loubet, B.,

330 Altimir, N., Gruenhage, L., Ammann, C., Cieslik, S., Paoletti, E., Mikkelsen, T. N., Ro-Poulsen, H., Cellier, P., Cape, J. N., Horvath, L., Loreto, F., Niinemets, U., Palmer, P. I., Rinne, J., Misztal, P., Nemitz, E., Nilsson, D., Pryor, S., Gallagher, M. W., Vesala, T., Skiba, U., Brueggemann, N., Zechmeister-Boltenstern, S., Williams, J., O'Dowd, C., Facchini, M. C., de Leeuw, G., Floss- man, A., Chaumerliac, N., and Erisman, J. W.: Atmospheric com- position change: Ecosystems-Atmosphere interactions, Atmos. Environ., 43, 5193–5267, doi:10.1016/j.atmosenv.2009.07.068, 2009.

335 Gerharz, L., Gräler, B., and Pebesma, E.: Measurement artefacts and inhomogeneity detection, technical report, Uni. Münster, Germany, under subcontract of ETC/ACM Consortium institute RIVM, ETC/ACM, 54 pp, 2011.

Hogrefe, C., Rao, S. T., Zurbenko, I. G., and Porter, P. S.: Interpreting the Information in Ozone Observations and Model Predictions Relevant to Regulatory Policies in the Eastern United States, 1999.

Hogrefe, C., Roselle, S., Mathur, R., Rao, S. T., and Galmarini, S.: Space-time analysis of the Air Quality Model Evaluation

340 International Initiative (AQMEII) Phase 1 air quality simulations, J. Air Waste Manag. Assoc., 64, 388–405, https://doi.org/10.1080/10962247.2013.811127, 2014.

Huijnen, V., Miyazaki, K., Flemming, J., Inness, A., Sekiya, T., and G. Schultz, M.: An intercomparison of tropospheric ozone reanalysis products from CAMS, CAMS interim, TCR-1, and TCR-2, Geosci. Model Dev., 13, 1513–1544, https://doi.org/10.5194/gmd-13-1513-2020, 2020.

345   Inness, A., Ades, M., Agustí-Panareda, A., Barr, J., Benedictow, A., Blechschmidt, A. M., Jose Dominguez, J., Engelen, R., Eskes, H., Flemming, J., Huijnen, V., Jones, L., Kipling, Z., Massart, S., Parrington, M., Peuch, V. H., Razinger, M., Remy, S., Schulz, M., and Suttie, M.: The CAMS reanalysis of atmospheric composition, Atmos. Chem. Phys., 19, 3515–3556, https://doi.org/10.5194/acp-19-3515-2019, 2019.

Jafari, F. and Farshad, H.: Synoptic analysis of the most durable pollution and clean waves during 2009 – 2019 in Tehran City
350   (capital of Iran), Nat. Hazards, 110, 1247–1272, https://doi.org/10.1007/s11069-021-04990-5, 2022.

Kaffashzadeh, N.: A Statistical Analysis of Surface Ozone Variability Over the Mediterranean Region During Summer, Ph.D. thesis, Rheinishe Friedrich-Wilhelms-Universität Bonn, Germany, https://nbn-resolving.org/urn:nbn:de:hbz:5n-52000, 130 pp., 2018.

Kang, D., Hogrefe, C., Foley, K. L., Napelenok, S. L., Mathur, R., and Rao, S. T.: Application of the Kolmogorov Zurbenko
355   filter and the decoupled direct 3D method for the dynamic evaluation of a regional air quality model, Atmos. Environ., 80, 58–69, https://doi.org/10.1016/j.atmosenv.2013.04.046, 2013.

Lashkari, H., Keikhosravi, G., and Karimian, N.: Investigating Patterns of Severe Air Pollution in the Lower Tropospheric Layer of Tehran Metropolish, J. Geogr. Environ. Hazards, 9, 1–20, https://doi.org/10.22067/geo.v9i3.87260, 2020.

Lelieveld, J., Hoor, P., Jöckel, P., Pozzer, A., Hadjinicolaou, P., Cammas, J. P., and Beirle, S.: Severe ozone air pollution in
360   the Persian Gulf region, Atmos. Chem. Phys., 9, 1393–1406, https://doi.org/10.5194/acp-9-1393-2009, 2009.

Li, K., Jacob, D. J., Shen, L., Lu, X., Smedt, I. De, and Liao, H.: Increases in surface ozone pollution in China from 2013 to 2019: anthropogenic and meteorological influences, 20, 11423–11433, https://doi.org/10.5194/acp-20-11423-2020, 2020.

Lin, J. T., Youn, D., Liang, X. Z., and Wuebbles, D. J.: Global model simulation of summertime U.S. ozone diurnal cycle and its sensitivity to PBL mixing, spatial resolution, and emissions, 41, 36, 8470–8483,
365   https://doi.org/10.1016/j.atmosenv.2008.08.012, 2008a.

Lin, J., Wuebbles, D. J., and Liang, X.: Effects of intercontinental transport on surface ozone over the United States: Present and future assessment with a global model, 35, 1–6, https://doi.org/10.1029/2007GL031415, 2008b.

Loneck, B., and Zurbenko, I.: Theoretical and Practical Limits of Kolmogorov-Zurbenko Periodograms with DiRienzo-Zurbenko Algorithm Smoothing in the Spectral Analysis of Time Series Data Barry, arXiv [preprint], arXiv:2007.03031v1,
370   28 pp., 2020.

Schulz, M., Q. Errera, M. Ramonet, Sudarchikova, N., H. J. Eskes, S. Basart, A. Benedictow, Y. Bennouna, A.-M. Blechschmidt, S. Chabrillat, Christophe, Y., E. Cuevas, A. El-Yazidi, H. Flentje, P. Fritzsche, K.M. Hansen, U. Im, J. Kapsomenakis, B. Langerock, A. Richter, V. Thouret, A. Wagner, T. Warneke, C. Zerefos, Validation report of the CAMS near-real-time global atmospheric composition service: Period December 2020 – February 2021, Copernicus Atmosphere
375   Monitoring Service (CAMS) report, CAMS84_2018SC3_D1.1.1_DJF2021.pdf, doi:10.24380/ f540-kb09, 190 pp., June 2021.

Malley, C. S., Heal, M. R., Mills, G., and Braban, C. F.: Trends and drivers of ozone human health and vegetation impact metrics from UK EMEP supersite measurements (1990 – 2013), 4025–4042, https://doi.org/10.5194/acp-15-4025-2015, 2015.

Mills, G., Hayes, F., Simpson, D., Emberson, L., Norris, D., Har- mens, H., and Büker, P.: Evidence ofwidespread effects ofozone on crops and (semi-)natural vegetation in Europe (1990–2006) in relation to AOT40-and flux-based risk maps, Global.

380   Change. Biol., 17, 592–613, https://doi.org/10.1111/j.1365-2486.2010.02217.x, 2011.

Monks, P. S., Archibald, A. T., Colette, A., Cooper, O., Coyle, M., Derwent, R., Fowler, D., and Granier, C.: Tropospheric ozone and its precursors from the urban to the global scale from air quality to short-lived climate forcer, 8889–8973, https://doi.org/10.5194/acp-15-8889-2015, 2015.

Ordónez, C., Mathis, H., Furger, M., Henne, S., Hüglin, C., Staehelin, J., and Prévǒt, A. S. H.: Changes of daily surface ozone

385   maxima in Switzerland in all seasons from 1992 to 2002 and discussion of summer 2003, Atmos. Chem. Phys., 5, 1187–1203, https://doi.org/10.5194/acp-5-1187-2005, 2005.

Otero, N., Sillmann, J., Mar, K. A., Rust, H. W., Solberg, S., Andersson, C., Engardt, M., Bergström, R., Bessagnet, B., Colette, A., Couvidat, F., Cuvelier, C., Tsyro, S., Fagerli, H., Schaap, M., Manders, A., and Mircea, M.: A multi-model comparison of meteorological drivers of surface ozone over Europe, 18, 12269–12288, https://doi.org/10.5194/acp-18-12269-2018, 2018.

390   Otero, N., Sillmann, J., Schnell, J. L., Rust, H. W., and Butler, T.: Synoptic and meteorological drivers of extreme ozone concentrations over Europe Synoptic and meteorological drivers of extreme ozone concentrations over Europe, Environ. Res. Lett. 11 024005, 2016.

Park, S., Son, S. W., Jung, M. Il, Park, J., and Park, S. S.: Evaluation of tropospheric ozone reanalyses with independent ozonesonde observations in East Asia, Geosci. Lett., 7, https://doi.org/10.1186/s40562-020-00161-9, 2020.

395   Rao, S. T., Zurbenko, I. G., Neagu, R., Porter, P. S., Ku, J. Y., and Henry, R. F.: Space and Time Scales in Ambient Ozone Data, Bulletin of the American Meteorological Society, 78, 10, 2153–2166, https://doi.org/10.1175/1520-0477(1997)078<2153:SATSIA>2.0.CO;2, 1997.

Rasmussen, D. J., Fiore, A. M., Naik, V., Horowitz, L. W., McGin- nis, S. J., and Schultz, M. G.: Surface ozone-temperature relationships in the eastern US: A monthly climatology for evalu-ating chemistry-climate models, Atmos. Environ., 47, 142–

400   153, https://doi.org/10.1016/j.atmosenv.2011.11.021, 2012.

Seo, J., Youn, D., Kim, J. Y., and Lee, H.: Extensive spatiotemporal analyses of surface ozone and related meteorological variables in South Korea for the period 1999 – 2010, 6395–6415, https://doi.org/10.5194/acp-14-6395-2014, 2014.

Solazzo, E. and Galmarini, S.: Error apportionment for atmospheric chemistry-transport models – a new approach to model evaluation, 6263–6283, https://doi.org/10.5194/acp-16-6263-2016, 2016.

405   Stevenson, D. S., Dentener, F. J., Schultz, M. G., Ellingsen, K., van Noije, T. P. C., Wild, O., Zeng, G., Amann, M., Atherton, C. S., Bell, N., Bergmann, D. J., Bey, I., Butler, T., Cofala, J., Collins, W. J., Derwent, R. G., Doherty, R. M., Drevet, J., Eskes, H. J., Fiore, A. M., Gauss, M., Hauglustaine, D. A., Horowitz, L. W., Isaksen, I. S. A., Krol, M. C., Lamarque, J. F., Lawrence, M. G., Montanaro, V., Müller, J. F., Pitari, G., Prather, M. J., Pyle, J. A., Rast, S., Rodriquez, J. M., Sanderson, M. G., Savage,

N. H., Shindell, D. T., Strahan, S. E., Sudo, K., and Szopa, S.: Multimodel ensemble simulations of present-day and near-
410   future tropospheric ozone, J. Geophys. Res. Atmos., 111, https://doi.org/10.1029/2005JD006338, 2006.

Sudarchikova, N., M. Schulz, Q. Errera, M. Ramonet, H. J. Eskes, S. Basart, A. Benedictow, Y. Bennouna, A.-M.
Blechschmidt, S. Chabrillat, Christophe, Y., E. Cuevas, A. El-Yazidi, H. Flentje, P. Fritzsche, K.M. Hansen, U. Im, J.
Kapsomenakis, B. Langerock, A. Richter, V. Thouret, A. Wagner, T. Warneke, C. Zerefos, Validation report of the CAMS
near-real-time global atmospheric composition service: Period September - November 2020, Copernicus Atmosphere
415   Monitoring Service (CAMS) report, CAMS84_2018SC3_D1.1.1_SON2020.pdf, doi: 10.24380/ rysv-7371, 159 pp., March
2021.

Taylor: Automated quality control methods for sensor data: a novel observatory approach, 4957–4971,
https://doi.org/10.5194/bg-10-4957-2013, 2013.

Tyrlis, E., Lelieveld, J., and Steil, B.: The summer circulation over the eastern Mediterranean and the Middle East: influence
420   of the South Asian monsoon, 1103–1123, https://doi.org/10.1007/s00382-012-1528-4, 2013.

Wang, Y., Ma, Y., Eskes, H., Inness, A., Flemming, J., and Brasseur, G. P.: Evaluation of the CAMS global atmospheric trace
gas reanalysis 2003 – 2016 using aircraft campaign observations, Atmos. Chem. Phys., 20, 4493–4521,
https://doi.org/10.5194/acp-20-4493-2020, 2020.

Yang, W. and Zurbenko, I.: Kolmogorov – Zurbenko filters, https://doi.org/10.1002/wics.71, 2010.

425   Yousefian, F., Faridi, S., Azimi, F., Aghaei, M., Shamsipour, M., Yaghmaeian, K., and Hassanvand, M. S.: Temporal variations
of ambient air pollutants and meteorological influences on their concentrations in Tehran during 2012–2017, Sci. Rep., 10, 1–
11, https://doi.org/10.1038/s41598-019-56578-6, 2020.

Zahumenský, I.: Guidelines on Quality Control Procedures for Data from Automatic Weather Stations Guidelines on Quality
Control Procedures for Data from Automatic Weather Stations, World Meteorological Organization, 10 pp., 2004.

430   Zohdirad, H., Montazeri Namin, M., Ashrafi, K., Aksoyoglu, S., and Prévôt, A. S. H.: Temporal variations, regional
contribution, and cluster analyses of ozone and NOx in a middle eastern megacity during summertime over 2017–2019,
Environ. Sci. Pollut. Res., 29, 16233–16249, https://doi.org/10.1007/s11356-021-14923-1, 2022.

Zurbenko, I., Porter, P. S., Gui, R., Rao, S. T., Ku, J. Y., & Eskridge, R. E.: Detecting discontinuities in time series of upper-
air data: development and demonstration of an adaptive filter technique, Journal of Climate, 9, 12, 3548-3560,
435   https://doi.org/10.1175/1520-0442(1996)009<3548:DDITSO>2.0.CO;2, 1996.
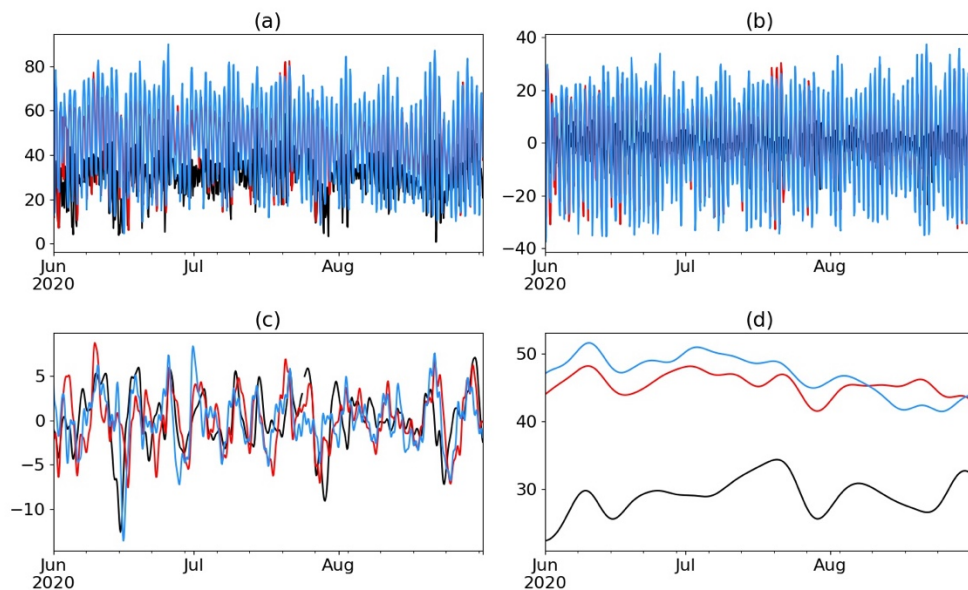
Figure 1. It shows different spectral components of O$_3$ for dfo (black), dfr (red) and dfa (blue) at station 1 for JJA. (a) presents the original time series and (b), (c) and (d) are short (S), medium (M) and long range (L) fluctuation terms, respectively. The vertical axis in all panels show ozone mixing ratio in nmol mol^{-1}.

440

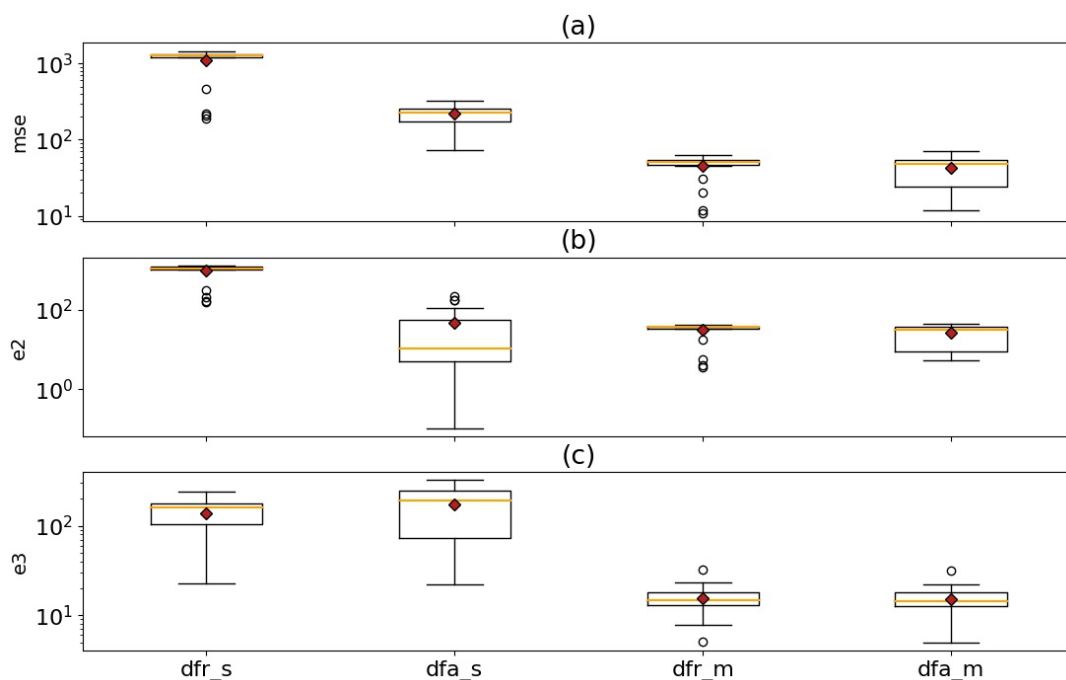**Figure 2. This figure shows the (a) MSE, (b) e$_2$, and (c) e$_3$ of dfr, and dfa for both S and M components of O$_3$. In this figure, dfr_s and dfa_s refer to the S component of dfr and dfa, respectively. Likewise, dfr_m and dfa_m refer to the M component of dfr and dfa, respectively.**
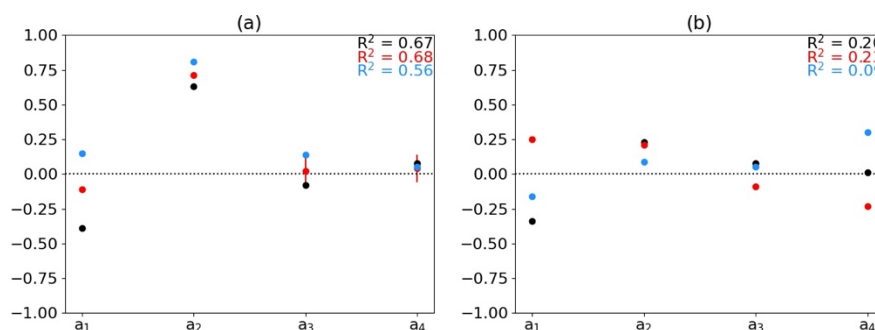
445

Table 1. The regression coefficients, i.e., a_1, a_2, a_3, and a_4, and coefficients of determination, i.e., R^2, for S and M components of dfo dataset at station 8.

component	S		M	
a_1	-0.39	0.01	-0.34	0.02
a_2	0.63	0.02	0.23	0.02
a_3	-0.08	0.01	0.08	0.02
a_4	0.08	0.01	0.01	0.02
R^2	0.67		0.20	

450

Figure 3. This figure shows regression coefficient of (a) S and (b) M components for dfo (black), dfr (red) and dfa (blue) datasets at station 8.

455

Appendix A

Table A1. Characteristics of the stations.

Number	Name	Latitude	Longitude	Altitude	Model level
1	Abresan (Tabriz)	38.066	46.326	1440	137
2	Namaz square (Tabriz)	38.079	46.289	1393	137
3	Azarbayejan square (Tabriz)	38.112	46.276	1362	137
4	Aqdasiyeh (Tehran)	35.795	51.484	1528	123
5	Sadr (Tehran)	35.778	51.429	1488	124
6	District 2 (Tehran)	35.777	51.368	1559	123
7	Punak (Tehran)	35.762	51.332	1468	124
8	Geophysics (Tehran)	35.74	51.385	1368	126
9	Setad bohran (Tehran)	35.727	51.431	1284	129
10	Tarbiat Modares (Tehran)	35.717	51.386	1264	129
11	Sharif university (Tehran)	35.702	51.351	1187	132
12	District 21 (Tehran)	35.698	51.243	1219	131

13	Piroozi (Tehran)	35.696	51.494	1209	131
14	Fath square	35.679	51.337	1151	133
15	Shad abad (Tehran)	35.67	51.297	1157	133
16	Mahallati (Tehran)	35.661	51.466	1139	134
17	District 19 (Tehran)	35.635	51.362	1103	135
18	Masoudieh (Tehran)	35.63	51.499	1177	136
19	Ray	35.604	51.426	1065	137

460

Table A2. The standard deviation for the S component of the variables at station 8.

Variables	O_3	NO_x	AT	WS	WD
dfo	18.11	43.36	2.76	0.87	42.77
dfr	44.93	82.33	2.69	0.55	66.07
dfa	19.09	392.44	2.88	0.69	79.76

465

Table A3. The standard deviation for the M component of the variables at station 8.

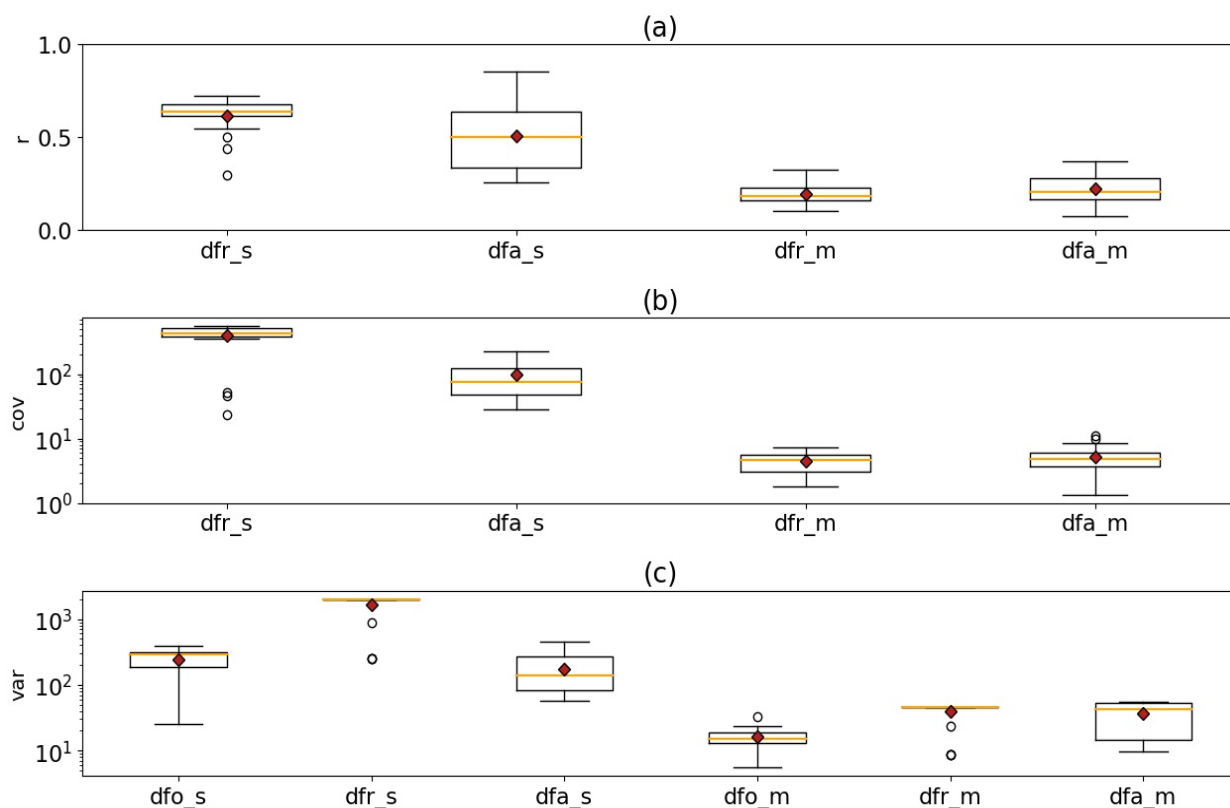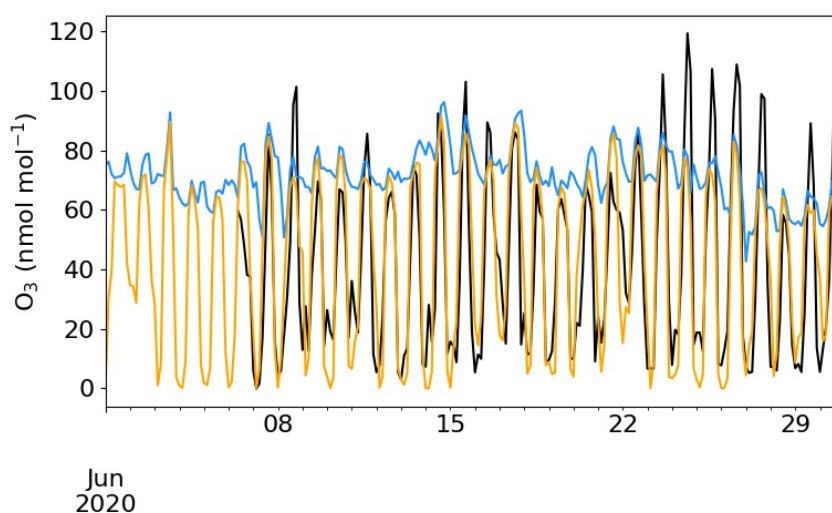| Variables	O_3	NO_x	AT	WS	WD
dfo	4.88	20.89	1.59	0.38	21.84
dfr	6.83	28.39	1.43	0.36	44.91
dfa	2.5	202.41	1.43	0.41	60.16

470

Figure A1. The (a) correlation, (b) covariance, and (c) variance of the simulated O_3 in dfr, and dfa for both S and M components.

475

Figure A2. The O_3 time series for June 2020 at station 4. The black line shows observations (dfo) and orange and blue colours show dfa in two different model levels, i.e., 137 and 123, respectively.
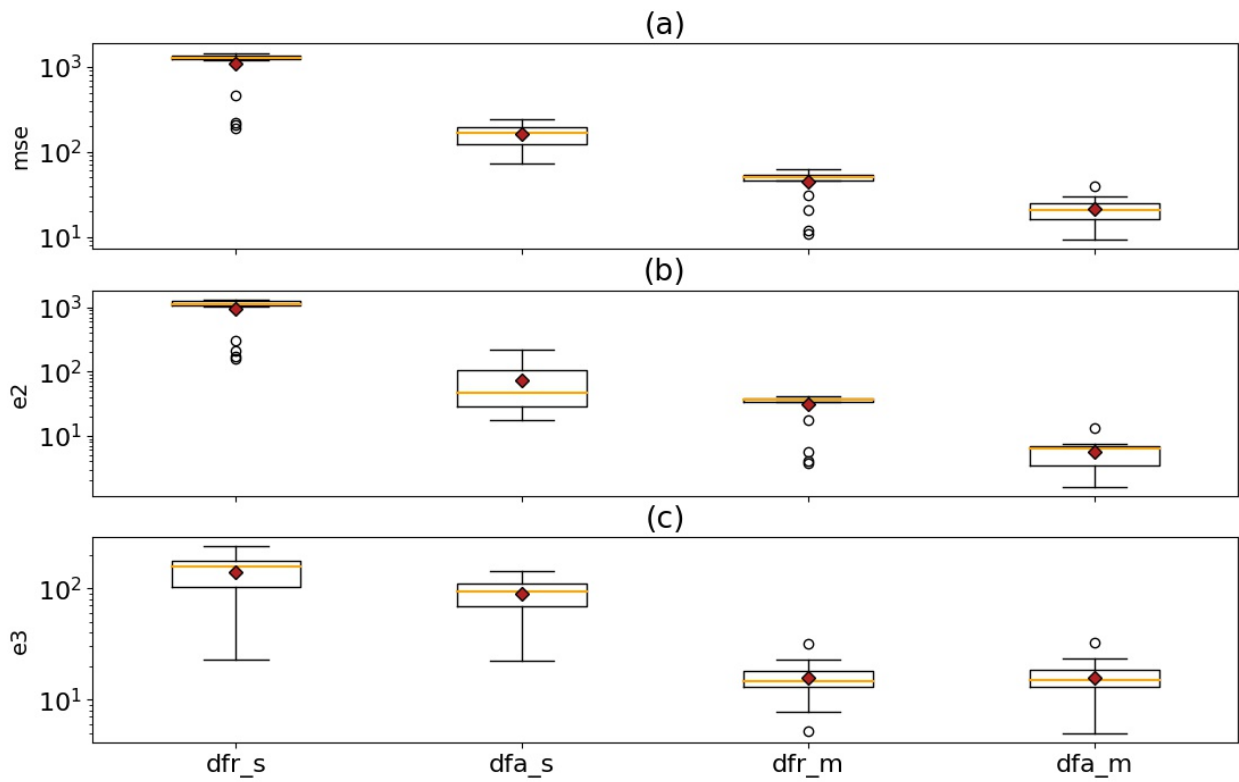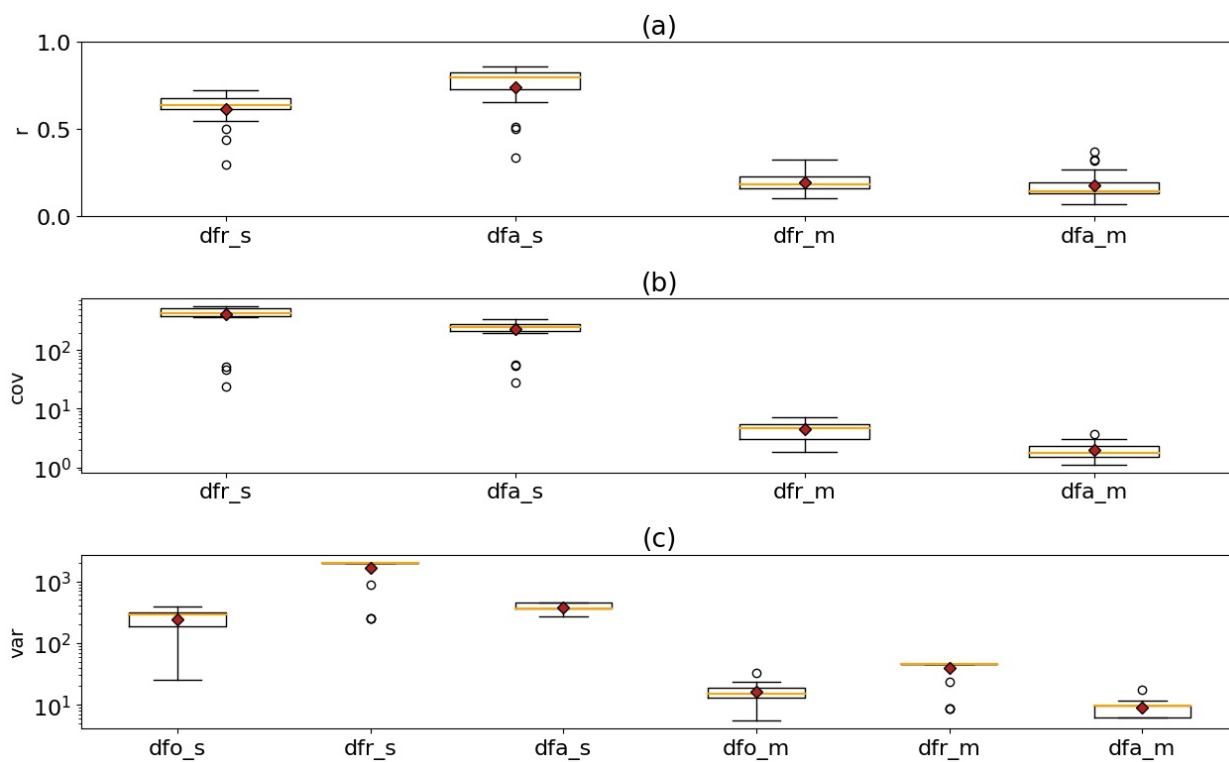
Geoscientific
Model Development
Discussions

Figure A3. Similar to Fig. 2, but here the surface level is used as a vertical model level, i.e., lev = 60 for dfr and lev = 137 for dfa.

480

Figure A4. Similar to Fig. A1, but here the surface level is used as a vertical model level, i.e., lev = 60 for dfr and lev = 137 for dfa.